

Article

# Photocatalytic Efficacy and Degradation Kinetics of Chitosan-Loaded Ce-TiO<sub>2</sub> Nanocomposite towards for Rhodamine B Dye

Anish Clastin Indira <sup>1</sup>, Jaya Rajan Muthaian <sup>1,\*</sup>, Muthirulan Pandi <sup>2</sup>, Faruq Mohammad <sup>3,\*</sup>, Hamad A. Al-Lohedan <sup>3</sup> and Ahmed A. Soleiman <sup>4</sup>

- <sup>1</sup> Department of Chemistry & Research, Annai Velankanni College, Tholayavattam-629157, Affiliated to Manonmanium Sundarnar University, Tirunelveli 627012, Tamil Nadu, India
- <sup>2</sup> Department of Chemistry, Lekshmipuram of College Arts and Science, Neyyoor-629802, Affiliated to Manonmanium Sundarnar University, Tirunelveli 627012, Tamil Nadu, India; pmuthirulan@gmail.com
- <sup>3</sup> Department of Chemistry, College of Science, King Saud University, P.O. Box 2455, Riyadh 11451, Saudi Arabia; hlohedan@ksu.edu.sa
- <sup>4</sup> College of Sciences and Engineering, Southern University, Baton Rouge, LA 70813, USA
- \* Correspondence: jayarajanm1983@gmail.com (J.R.M.); fmohammad@ksu.edu.sa (F.M.); Tel.: +966-(0)-114675998 (F.M.)

**Abstract:** The recent advancement in the production of nanomaterials with novel architectures and functionality has allowed for the effective treatment of industrial wastewaters and contaminated soil and, in that view, the current study aimed to investigate the catalytic efficacy of biopolymer-loaded titanium nanocomposite. Therefore, Cerium (Ce)-titanium dioxide (TiO<sub>2</sub>) loaded chitosan nanocomposite was formed and studied its catalytic efficacy towards the degradation of an industrial dye pollutant. For the production of Ce-TiO<sub>2</sub>/chitosan nanocomposite, we followed the hydrothermal synthesis route and the formed nanocomposite was thoroughly analyzed for the crystallinity (using powdered X-ray diffraction, XRD), surface bonding, and nature (using Fourier transform infrared, FTIR spectroscopy), morphology (scanning electron microscopy, SEM), elemental composition (electron diffraction analysis by X-rays, EDAX), porosity (Brunauer–Emmett–Teller, BET), and particles size in powdered form (transmission electron microscopy, TEM). Then the efficiency of synthesized nanocomposite was tested towards the photocatalytic degradation of Rhodamine B (Rh B) dye by applying various parameters such as the irradiation time, solution pH, catalyst dosage, and the dye concentration. Further, the Langmuir–Hinshelwood model was employed to investigate the kinetics of RhB degradation and provided a conceivable photocatalytic mechanism. It was indicated based on the catalyst mechanism that the modification of TiO<sub>2</sub> nanoparticles with Ce and loading onto chitosan biopolymer may have accelerated the photocurrent transport due to an increase in the number of electrons and holes generated by the photon's irradiation. In this way, the study has witnessed the excellent photocatalytic performance of Ce-TiO<sub>2</sub>/chitosan with 95% Rh B degradation as against the pure TiO<sub>2</sub> nanoparticles thus stressing the importance of developing novel composite photocatalysts.

**Keywords:** photodegradation; nanocomposite formation; TiO<sub>2</sub> catalysis; langumir-heinshelwood; UV irradiation; wastewater treatment



**Citation:** Clastin Indira, A.; Muthaian, J.R.; Pandi, M.; Mohammad, F.; Al-Lohedan, H.A.; Soleiman, A.A. Photocatalytic Efficacy and Degradation Kinetics of Chitosan-Loaded Ce-TiO<sub>2</sub> Nanocomposite towards for Rhodamine B Dye. *Catalysts* **2023**, *13*, 1506. <https://doi.org/10.3390/catal13121506>

Academic Editors: Maria Laura Tummino, Rufino Navarro Yerga and Jorge Bedia

Received: 16 October 2023

Revised: 1 December 2023

Accepted: 8 December 2023

Published: 11 December 2023



**Copyright:** © 2023 by the authors. Licensee MDPI, Basel, Switzerland. This article is an open access article distributed under the terms and conditions of the Creative Commons Attribution (CC BY) license (<https://creativecommons.org/licenses/by/4.0/>).

## 1. Introduction

Water and soil contamination associated with environmental pollution are serious concerns across the globe and it requires immediate action to incorporate sustainable development [1]. One of the major sources of this water, soil, and air contamination are the industries, and in particular, the metal, wood, paint, and textile plants that use synthetic dyes for coloring. For the textile industry alone, more than 10,000 tons of dyes are used all over the globe annually, and the fabrics consume only 70–80% while the remaining 20% of

dye effluent causes severe environmental issues [2]. This unused/remaining dye effluent in its untreated form from the industries affects the aquatic ecosystem by flowing toward water bodies like ponds, rivers, and lakes. The commonly used synthetic dyes include azo dye, ramazol orange, rhodamine, methylene blue, etc., which are mostly carcinogenic to humans as they are all very difficult to remove from the water bodies. Apart from the persistence of dye molecules in the water streams, the dye removal process is tedious and associated with high costs and low efficiency [3,4].

The commonly employed physico-chemical methods for the removal of organic dye pollutants from industrial and agriculture effluents include adsorption, electrocoagulation, nano/ultra-membrane filtration, reverse osmosis, ion exchange, etc. [5]. However, the compromised ability of these conventional wastewater treatment technologies is demanding the development of sustainable, economical, environmentally friendly, feasible, and highly effective plants that can fully eliminate the dye contaminants [6]. To resolve this problem, water purification processes are applied at which cost-effective and eco-friendly techniques are most essential in treating the polluted wastewater. In that view, the photocatalytic dye degradation technique has been identified to be the sophisticated one because of its low-cost, ecofriendly nature, efficacy, and easy processing. This method acts by generating highly active reactive species following the UV-light irradiation from sunlight [7,8].

Heterogeneous photocatalysis with semiconductor nanoparticles serves as an alternative and exceptionally effective technique, where the mechanism proceeds through the generation of highly reactive hydroxyl free radical oxidants. In the following step, the formed free radicals reacted with the noxious pollutant dye molecules and reduced the concentration of organic compounds [9]. Hence many different catalysts are being tested in this direction like the metallic oxides (Ta, Sr, Cd, Zn, Ti, etc.), and among all, titanium dioxide ( $\text{TiO}_2$ ) has a special role in the photocatalysis sector particularly decomposing synthetic dyes because of its abundance and low cost, high efficacy, immune to chemical corrosion, and long-term stability. In that view, various  $\text{TiO}_2$ -based photocatalysts are being developed with a change of doping agent, conjugation, surface functionality, etc., as these additional groups help to further enhance the light-harvesting ability, photochemical reactivity, aquatic stability, and minimize the environmental toxicity [10,11].

$\text{TiO}_2$  is an active photocatalyst, although various changes (doping) and combinations (conjugation/loading) are being applied to make it further efficient, the rapid charge recombination ability mainly limits its potentiality during the photocatalytic degradation pathways [12]. As this dynamic charge, recombination is strongly influenced by the structure, shape, and optical properties and the  $\text{TiO}_2$  modification must be applied in a way that increases photogenerated charge carrier separation efficiency to ameliorate the photocatalytic capacity [13]. Such a valence electronic transformation in the atomic structure can maintain the  $\text{TiO}_2$  nanocomposite as a superior candidate for organic dye degradation reactions which are influenced by light irradiation.

One approach to slow down the rate of charge carrier recombination involves the use of metal doping as it helps to create hetero-junctions between the two semiconductors. In that view, various studies are being carried out by the doping of single or multiple metal ions (like Zn, Cd, Mn, Cu, etc.) with  $\text{TiO}_2$  nanoparticles as the combination increases the electronic band gap and prevents the charge scavenging capacity to support an improved photocatalytic activity. One of the studies provides information that the  $\text{TiO}_2$  nanoparticle's interaction with that of rare-earth metals, in particular, the cerium (Ce) metal can improve the photocatalytic performance significantly. This enhancement is attributed to the formation of Lewis base complexes originating from the d-orbital interaction with that of f-orbital functional groups of rare earth metals. In addition, the availability of higher surface sites for suitable ions doped into the host lattice boosts the electron trapping, and the difference in band gap energy supports for an increased photocatalytic activity [14].

In addition, the problems arising from the powdered form of  $\text{TiO}_2$  like the recovery, unwanted toxicity (due to the nanosized particles), high agglomeration, and difficulty of thin film formation are identified to be relieved through the combination of  $\text{TiO}_2$  with

chitosan biopolymer. Such developed Chitosan-TiO<sub>2</sub> composites are investigated to possess a high rate of flexibility, formation into a range of thicknesses, and light harvesting capacity. Also, the chitosan biopolymer offers continuous and stable support to fully adsorb the dye molecules that need to be degraded by the TiO<sub>2</sub> catalyst, and in this way, the recombination can easily be dodged [15]. Moreover, taking advantage of the pH-responsive nature of chitosan biopolymer, many different pollutants like heavy metals, and organic and inorganic dyes are being successfully removed through surface adsorption from the wastewater.

By considering the abilities of Ce and the biopolymer of chitosan towards the production of an effective and stable photocatalyst, the present study aims to study the photocatalytic nature of a stable nanocomposite of Ce-TiO<sub>2</sub>/chitosan. We hypothesized that the loading of Ce-TiO<sub>2</sub> nanoparticles onto the biopolymer of chitosan serves to further improve the surface area, aqueous stability, surface functionality, and structural stability [16]. To the best of our knowledge, there have been only limited studies that are aimed at studying the dye degradation capacity of pure TiO<sub>2</sub>/Ce [17] and TiO<sub>2</sub>/chitosan nanocomposite [18], while no closer report investigates the photocatalytic degradation of Rhodamine B (RhB) dye involving the Ce-TiO<sub>2</sub>/chitosan composite. Therefore, the scope of the present investigation is to study the photocatalytic efficacy and degradation kinetics of RhB dye under the influence of Ce-TiO<sub>2</sub>/chitosan catalyst mediated by solar irradiation. For that, we first formed the nanocomposite by the hydrothermal synthesis route, and then fully analyzed the surface, morphological, optical, electronic, and elemental characteristics. Further, the RhB dye degradation and kinetics by altering the initial dye concentration, contact time, irradiation time, and solution pH are compared among pure TiO<sub>2</sub>, Ce-TiO<sub>2</sub>, and Ce-TiO<sub>2</sub>/chitosan, as the same methodology can be applied for the anchoring of other metal oxides onto biopolymer matrix.

## 2. Results and Discussion

### 2.1. Characterization of Ce-TiO<sub>2</sub>/Chitosan Nanocomposite

Figure 1A,B depicts the powdered X-ray diffraction (XRD) pattern of Ce-TiO<sub>2</sub> and Ce-TiO<sub>2</sub>/chitosan nanocomposite. From the diffraction pattern, the peaks of Ce-TiO<sub>2</sub> show peaks at  $2\theta = 27.5^\circ, 36.1^\circ, 37.9^\circ, 42^\circ, 54.1^\circ, 55.1^\circ, 62.7^\circ,$  and  $68.9^\circ$  indexed to 101, 004, 101, 105, and 211 planes (respectively), which can be attributed to the Anatase phase. Likewise, the Ce-TiO<sub>2</sub>/chitosan has diffraction peaks reflecting at the  $2\theta$  of  $25.3^\circ, 37.9^\circ, 48.1^\circ, 54.1^\circ, 62.7^\circ,$  and  $75^\circ$ , indicating for a well crystallized form. Also, it is very clear from the XRD pattern that the Ce-TiO<sub>2</sub>/chitosan composite has similar peaks to that of Ce-TiO<sub>2</sub> but with a slight reduction in the peak intensity followed by the disappearance of the diffraction peak of Chitosan. Additionally, it can be interesting to note that the final nano-composite structure of the Ce-TiO<sub>2</sub>/chitosan sample did not change much as compared to the native Ce-TiO<sub>2</sub> core, thereby confirming the maintenance of the same core characteristics and success of the synthesis procedure [19,20].

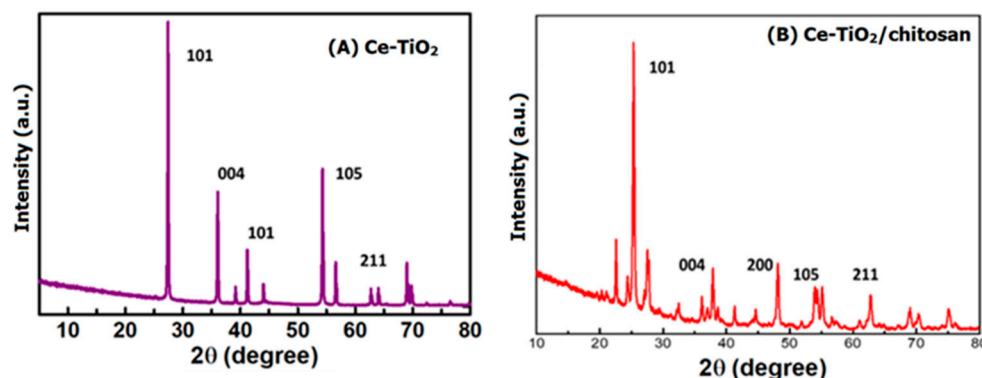
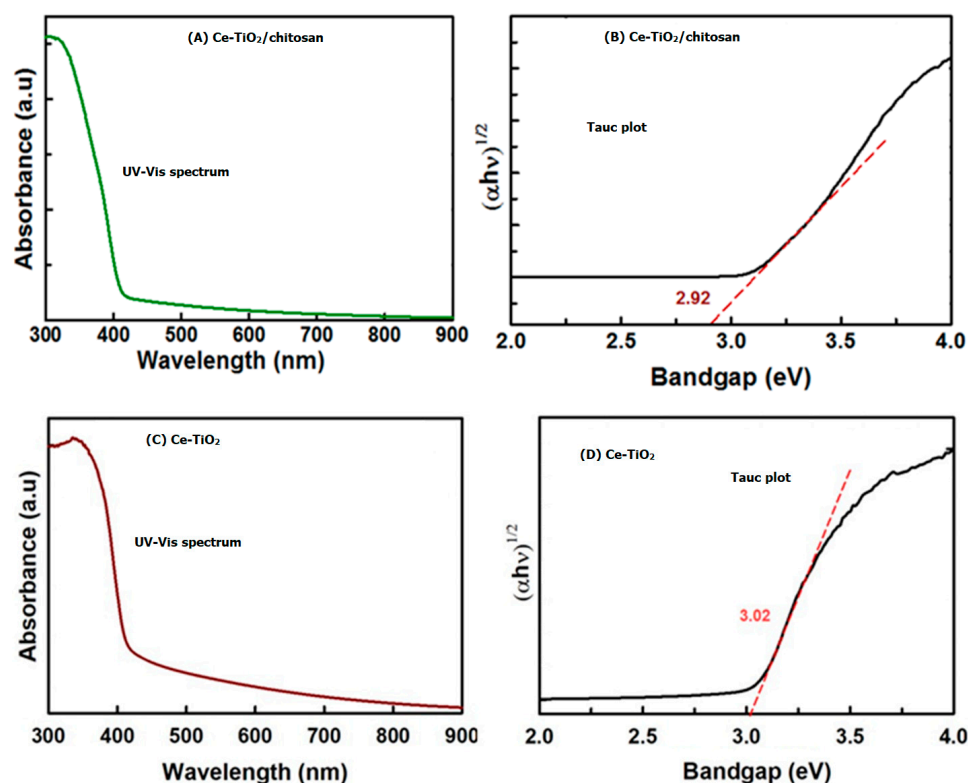


Figure 1. Powdered XRD analysis of Ce-TiO<sub>2</sub>(A) & Ce-TiO<sub>2</sub>/chitosan (B) nanocomposite.

The UV-Vis spectroscopy of as-synthesized Ce-TiO<sub>2</sub>/chitosan nanocomposite is provided in Figure 2A and from the graph, the sample exhibits an absorption band ranging from 300 to 450 nm which corresponds to the absorption property of a semiconductor material [20]. Also, the Ce-TiO<sub>2</sub>/chitosan nanocomposite absorption peak revealed that the chitosan loading can influence (in our case, reduce) TiO<sub>2</sub> nanoparticles absorption wavelength to a little extent. One possible explanation for such observation is that the chitosan molecules are in the vicinity of TiO<sub>2</sub>, allowing for the absorption and capturing of electrons nearby. In this way, chitosan availability can control the light energy required for the transition of electrons in TiO<sub>2</sub> and at the same time, reduces TiO<sub>2</sub>'s tendency of fast electron-hole recombination. Therefore, the observation of increased absorbance from the Ce-TiO<sub>2</sub>/chitosan nanocomposite material turned out to be due to chitosan presence which could also achieve improved absorption performance of TiO<sub>2</sub> to some extent, where they all can affect the photocatalytic property [21]. Further, Tauc's plot provided in Figure 2B indicates that the band gap energy of Ce-TiO<sub>2</sub>/chitosan nanocomposite is 2.92 eV. Tauc formula used to find the bandgap energy is:

$$(\alpha h\nu)^{\frac{1}{2}} = \beta(h\nu - E_g).$$

where  $E_g$  is the optical band gap,  $h$  the Planck's constant,  $\nu$  the incident photons,  $\beta$  a constant of the band tailing parameter, and  $\gamma$  is the index.



**Figure 2.** UV-Vis spectral analysis (A,C) and Tauc plots (B,D) of Ce-TiO<sub>2</sub>/chitosan nanocomposite and Ce-TiO<sub>2</sub> nanoparticles respectively.

The surface functionality and molecular nature of Ce-TiO<sub>2</sub> and Ce-TiO<sub>2</sub>/chitosan nano-composite were studied using the FTIR spectroscopy, where Figure 3A,B shows the FTIR spectra of Ce-TiO<sub>2</sub> and Ce-TiO<sub>2</sub>/chitosan nanocomposite respectively. From the spectrum, the Ce-TiO<sub>2</sub> (Figure 3A) composite contains two bands, one at 3265 cm<sup>-1</sup> and the other at 1618 cm<sup>-1</sup> which can be ascribed to the -OH stretching and bending vibration of adsorbed water molecules. Also, the other bands, 752 cm<sup>-1</sup> and 802 cm<sup>-1</sup> describe the characteristic peak of metal-oxygen, i.e., the Ti-O vibration [22,23]. However,

for the Ce-TiO<sub>2</sub>/chitosan nanocomposite (Figure 3B), the broad peak at 3285 cm<sup>-1</sup> is from the presence of N–H stretching. The absorption bands at 2957 cm<sup>-1</sup> and 2880 cm<sup>-1</sup> are ascribed to the alkyl C–H stretching and carboxylic O–H stretching vibrations. Similarly, the peak at 1636 cm<sup>-1</sup> ascribes the presence of amide from the chitosan molecules, and at the same time, the characteristic peaks at 1145 cm<sup>-1</sup> and 1037 cm<sup>-1</sup> corresponds to the C–N and C–O stretching vibrations. The peak at 743 cm<sup>-1</sup> from the Ti–O bond also persists in the nanocomposite, while the peaks appearing below 500 cm<sup>-1</sup> can be attributed to the Ti–O–Ce band, thereby confirming the successful formation of Ce-TiO<sub>2</sub>/chitosan nanocomposite [24,25]. Moreover, these characteristic peaks of the Ce-TiO<sub>2</sub>/chitosan nanocomposite indicate that the hydrogen bonding in chitosan molecules can become stronger following the formation of the Ce-TiO<sub>2</sub>/chitosan composite. Together with the TiO<sub>2</sub> metal oxide, the presence of amide, amine, and hydroxyl functional groups influence the physicochemical and architectural changes to the Ce-TiO<sub>2</sub>/chitosan composite that can aid in the efficient removal of dyes by photodegradation processes [26].

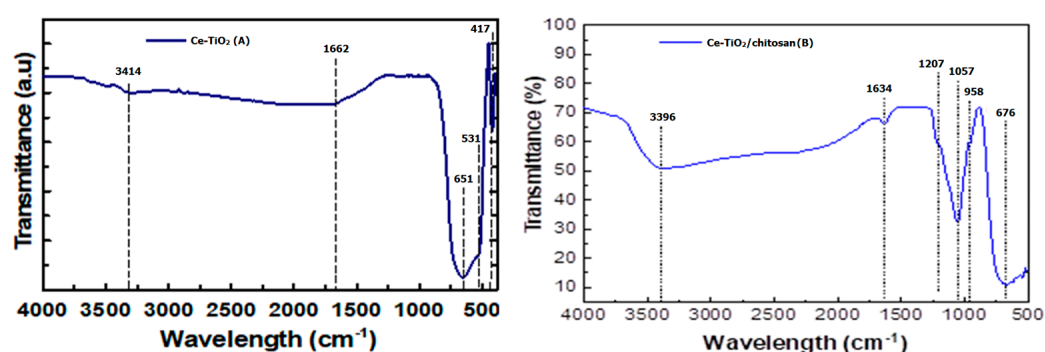
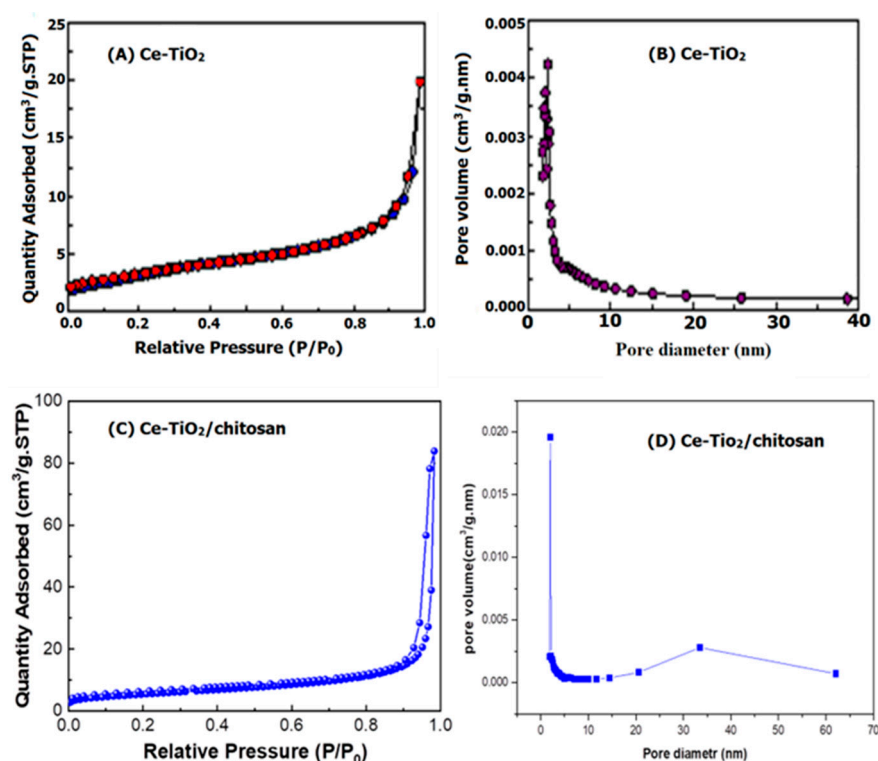


Figure 3. FT-IR spectral studies of Ce-TiO<sub>2</sub> (A) and Ce-TiO<sub>2</sub>/chitosan nanocomposite (B).

Brunauer-Emmett-Teller (BET) analysis was employed to investigate the specific surface area of the synthesized nanocomposite. Figure 4A–D compares the specific surface area of pure Ce-TiO<sub>2</sub>-Ce and Ce-TiO<sub>2</sub>/chitosan nanocomposite. The N<sub>2</sub> adsorption-desorption graph of Ce-TiO<sub>2</sub>/chitosan nanocomposite under low relative pressure ( $P/P_0$ ) conditions indicates the non-overlap of desorption graphs and this unusual case could occur with meta-stable agents like chitosan [26]. Such an observation can be attributed to the maintenance of interconnected pores by the composite and resembles a tinted bottle with evenly distributed pores. With this structure of nanocomposite, the process of desorption can occur through the percolation mechanism involving the outflow of gas phase from the pores [27]. Under low-pressure conditions, the re-strained/accumulated gasses in the sample pores can get released simultaneously, thereby resulting in an indication of desorbed gases than that of adsorbed in the adsorption–desorption graph. Although the other agents like TiO<sub>2</sub> and Ce are available, they are all covered by the chitosan biopolymer, where the pore volume and its average diameter were determined by the BET isotherm method and the values tabulated in Table 1. From the analysis, the specific surface area for the Ce-TiO<sub>2</sub>/chitosan composite was calculated to be 162 m<sup>2</sup>/g while for Ce-TiO<sub>2</sub> it is 114 m<sup>2</sup>/g [28].

Table 1. Pore volume and size of Ce-TiO<sub>2</sub> and Ce-TiO<sub>2</sub>/chitosan nanocomposite.

Sample	Surface Area (m <sup>2</sup> /g)	Pore Volume (cm <sup>3</sup> /g)	Pore Size (nm)
Ce-TiO <sub>2</sub> /chitosan	162	0.540	4.5955
Ce-TiO <sub>2</sub>	114	0.031	2.28



**Figure 4.** BET spectrums of Ce-TiO<sub>2</sub> (A) and Ce-TiO<sub>2</sub>/chitosan nanocomposite (C), and the corresponding pore diameter for Ce-TiO<sub>2</sub> (B) and Ce-TiO<sub>2</sub>/chitosan (D).

The surface morphology of the Ce-TiO<sub>2</sub>/chitosan nanocomposite is further confirmed by the FESEM analysis. Figure 5 shows the SEM image of Ce-TiO<sub>2</sub>/chitosan nanocomposite (A), compared to that of pure chitosan (B) and naked Ce-TiO<sub>2</sub> nanoparticles (C) at different magnifications. As observed from the FESEM of nanocomposite (Figure 5A), the chitosan biopolymer with its porous structure is completely covering the non-porous, crystalline Ce-TiO<sub>2</sub> nanoparticles (Figure 5C). All the single crystals of Ce-TiO<sub>2</sub> are mostly covered by the chitosan biopolymer in such a way that the Ce-TiO<sub>2</sub> nanoparticles have been fully distributed onto the matrices of chitosan. This conjugation has led to an improvement in the porosity and associated total surface area of nanocomposite as compared to the individual samples of naked Ce-TiO<sub>2</sub> and pure chitosan, thereby providing a solid support for the photocatalytic process to efficiently occur at its surface [29].

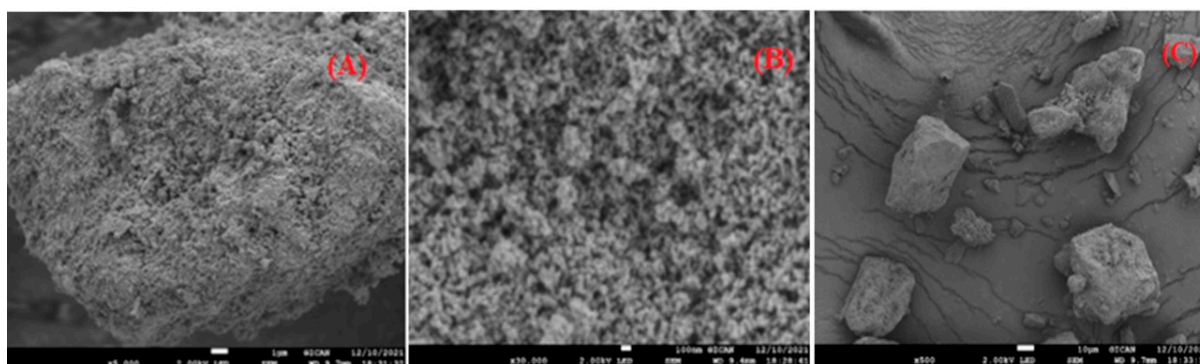


**Figure 5.** SEM images of Ce-TiO<sub>2</sub>/chitosan nanocomposite recorded at three different spots with varying magnifications (A–C).

The purity and elemental composition of as-prepared Ce-TiO<sub>2</sub>/chitosan nanocomposite was further confirmed by the electron diffraction analysis by X-rays (EDAX) spectra, where the analysis related to the elements of Ce, Ti, C, and O is provided in Figure 6. From

the graph, the appearance of elemental peaks at the respective positions confirms their availability in the nanocomposite. The analysis indicated that the weight percentage of Ce is 0.5%, Ti is 55.44%, C is 1.41%, and O is 39.81%. Table 2 denotes the elements present along with their weight percentages in the nanocomposite. In this, the availability of a high amount of Ti (more than 50%) within the stable chitosan matrix provides preliminary evidence for the potential effects of photocatalysis mediated by the Ti element [30].

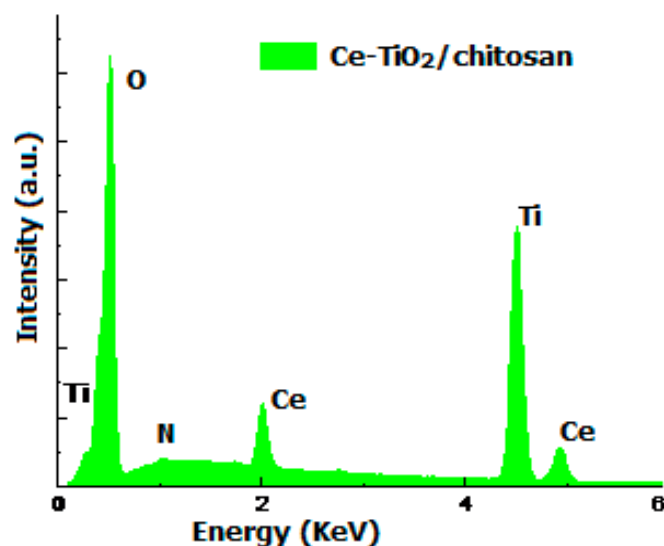


Figure 6. EDAX spectra of Ce-TiO<sub>2</sub>/chitosan nanocomposite.

Table 2. EDAX of Ce-TiO<sub>2</sub>/chitosan nanocomposite.

Element	Energy (keV)	Mass %	Atom %
C	0.277	1.41	3.04
O	0.525	39.81	64.49
P	2.013	2.85	2.38
Ti	4.508	55.44	30.00
Ce	4.837	0.50	0.09
Total		100.00	100.00

The Ce-TiO<sub>2</sub>/chitosan nanocomposite's morphological features were further examined by the TEM analysis and the particle image is shown in Figure 7. From the graph, the particles appear to be in uniform size and are fully agglomerated because of the availability of biopolymer of chitosan which has the nature of totally covering Ce/TiO<sub>2</sub> nanoparticles surfaces [31].

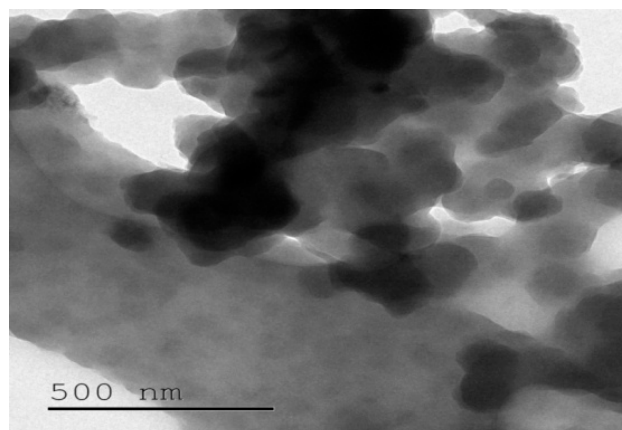
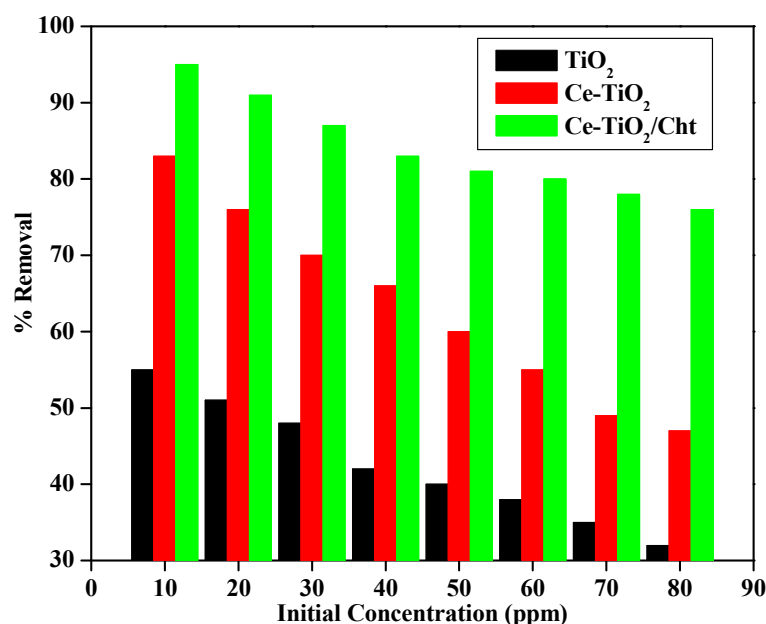


Figure 7. TEM image of Ce-TiO<sub>2</sub>/chitosan nanocomposite.

## 2.2. Photodegradation Studies

### 2.2.1. Influence of Dye Concentration and Contact Time

Studying the effects of the initial concentration of the photocatalyst material on dye degradation under light irradiation is essential for practical applications. Therefore, we investigated the photocatalytic behavior of  $\text{TiO}_2$ , and  $\text{Ce-TiO}_2$ , and compared them with that of  $\text{Ce-TiO}_2/\text{chitosan}$ . Figure 8 provides the comparative studies of RhB degradation under the photocatalytic influence of  $\text{TiO}_2$ ,  $\text{Ce-TiO}_2$ , and  $\text{Ce-TiO}_2/\text{chitosan}$  with constant catalyst amount (20 mg/100 mL), dye concentration range of 10 to 80 ppm, and irradiation time (80 min).



**Figure 8.** Comparison of the effects of changes in the initial RhB dye concentration (10–80 ppm) under UV irradiation of  $\text{Ce-TiO}_2/\text{chitosan}$  composite along with pure  $\text{TiO}_2$  and  $\text{Ce-TiO}_2$ .

From the graph, the percentage (%) degradation of RhB dye is decreasing significantly with that of an increased amount of initial dye concentration for all three catalysts ( $\text{TiO}_2$ ,  $\text{Ce-TiO}_2$ , and  $\text{Ce-TiO}_2/\text{chitosan}$ ). Such decreased catalytic activity has already been noticed in several investigations where the increase of target pollutant concentration leads to the adsorption of more and more molecules at the surface of the photocatalyst, causing a decrease in the light-harvesting ability and thus reduced photodegradation rate. The decreased photocatalytic activity may be due to (i) a very high concentration of dye molecules to serve as an inner filter that causes the diversion of incidence light photons at the catalyst surface, (ii) no or limited production of oxidative free radicals to participate in a catalyst mechanism, and (iii) blockage of active surface sites to participate in a catalytic reaction by the highly concentrated dye molecules [32]. Also, the results indicated that the  $\text{Ce-TiO}_2/\text{chitosan}$  composite possessed a higher efficiency towards the RhB dye degradation under UV light irradiation than the corresponding  $\text{Ce-TiO}_2$  and  $\text{TiO}_2$ . Such an observation may be from the combined effects of chitosan porosity, and its supportive nature to localize the dye molecules for longer periods.

### 2.2.2. Effect of Catalyst Dose on the Photocatalytic Degradation of RhB Dye

The optimization of catalyst amount and its dosage is very much necessary to avoid the usage of excess catalyst and at the same time, this ensures the complete absorption of irradiated light photons for effective photo mineralization. Also, the usage of optimal catalyst amount is governed by many different parameters like the reactor geometry, type of dye, its concentration, power of excitation source, and catalyst's definite amount.

Figure 9 compares the effect of Rh B dye degradation using  $\text{TiO}_2$ ,  $\text{Ce-TiO}_2$ , and  $\text{Ce-TiO}_2/\text{chitosan}$  when analyzed by varying the catalyst amounts and keeping other parame-

ters constant (initial dye concentration of 40 ppm, irradiation time of 90 min, and pH of 6.5) under UV irradiation. From the graph, the plot of % dye removal versus catalyst dose seems to be exponential towards RhB dye degradation for all the catalysts and among those three, the chitosan-based composite has very high activity followed by Ce-TiO<sub>2</sub> and the pure TiO<sub>2</sub> has the least activity. This increased activity at higher catalyst doses may be due to the availability of a greater number of active sites at the catalyst surface than that of dye molecules to undergo degradation. Also, in the case of a lower catalyst amount, the availability of limited active sites accessible at the adsorbent surface is needed when high dye molecules are present, resulting in a reduction of rapid solute adsorption. Moreover, it is to be pointed out that the catalyst dose significantly affects the number of active sites on the photocatalyst and the incident light penetration through the suspension [33]. A far increase in the total number of active sites may also cause a negative effect by decreasing the incident light penetration due to the strong shielding effect.

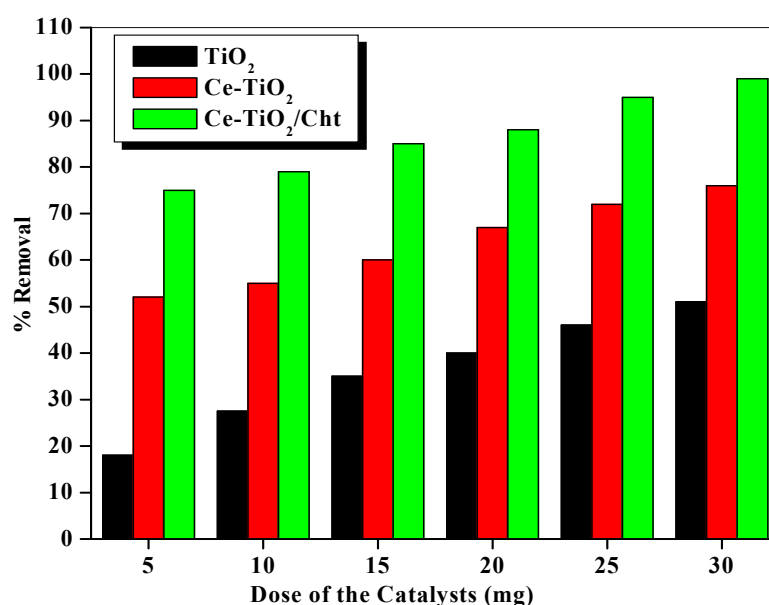


**Figure 9.** Comparison of % removal of RhB dye among the three different photocatalysts of TiO<sub>2</sub>, Ce-TiO<sub>2</sub>, and Ce-TiO<sub>2</sub>/chitosan as against the changes in catalyst dosage (5–30 mg).

### 2.3. Effect of Solution pH on RhB Degradation

The pH range of wastewater from the textile industry is typically very large. One of the most significant factors that affect the photo-oxidation processes and one that frequently affects dye wastewater properties is pH. Figure 10 compares the RhB dye degradation characteristics under varying pHs in the range of 3–8 with three different catalysts (TiO<sub>2</sub>, Ce-TiO<sub>2</sub>, Ce-TiO<sub>2</sub>/chitosan). For the photocatalytic reaction, all other experimental conditions were maintained constant like 40 ppm of initial dye concentration, 20 mg of catalyst, and 90 min of irradiation time.

As observed from the graph (Figure 10) the % of RhB dye decolorization is increased concerning an increase of solution pH for all three catalysts under UV light irradiations and very high for the Ce-TiO<sub>2</sub>/chitosan nanocomposite as compared to the other two. In general, TiO<sub>2</sub> possesses a 6.2 point of zero charges (PZC) and its surface gets positive charges accumulation under acidic conditions (pH < 6.2), while negative charges in the alkaline environments (pH > 6.2). However, RhB dye molecules possess positive charges because of the presence of amine groups in their structure and these groups get ionized in water solvent. The dye molecules in these ionic conditions possess electrostatic attraction towards the composite surface in the basic media and at the same time forbidden in the acidic media due to the columbic repulsion among the two positively charged TiO<sub>2</sub> particles and the dye molecules. Thus, the reaction rate of RhB dye degradation catalyzed by Ce-TiO<sub>2</sub>/chitosan reaches its maximum at a very high pH (i.e., basic environment) [34].

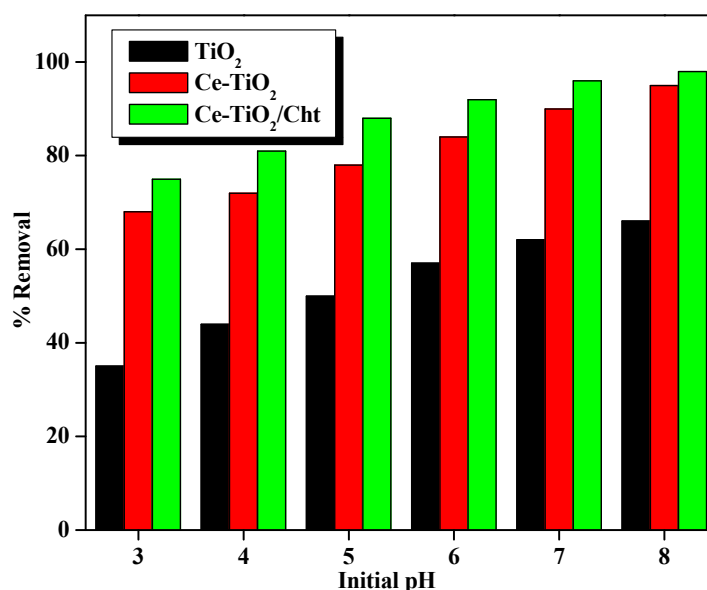


**Figure 10.** Comparison of % removal of RhB dye in the presence of three different catalysts under the influence of light irradiation with varying solution pHs.

#### 2.4. Effect of Irradiation Time on the RhB Dye Degradation

In general, for any photocatalytic reaction, the irradiation or contact time plays a very important role in the efficacy of the degradation process and so we have applied varied irradiation times for the decomposition of RhB dye. Figure 11 compares the RhB dye removal (standard of 40 ppm concentration) under the varying conditions of UV light irradiation times (viz., 10, 20, 30, 40, 50, 60, 70, 80, 90, and 100 min) with a constant catalyst dose of TiO<sub>2</sub>, Ce-TiO<sub>2</sub>, or Ce-TiO<sub>2</sub>/chitosan (20 mg per 100 mL). It has been observed from the graph that the photo decoloration (%) of RhB dye increases with time increase for all three catalysts and is very high for the Ce-TiO<sub>2</sub>/chitosan nanocomposite as against the other two. This observation can be linked to the high rate of light absorption originating from the chitosan presence in the nanocomposite in addition to the prolonged irradiation times, where this continuous absorption can efficiently break the dye molecules due to the action of electron-holes formation without undergoing any recombination [35].

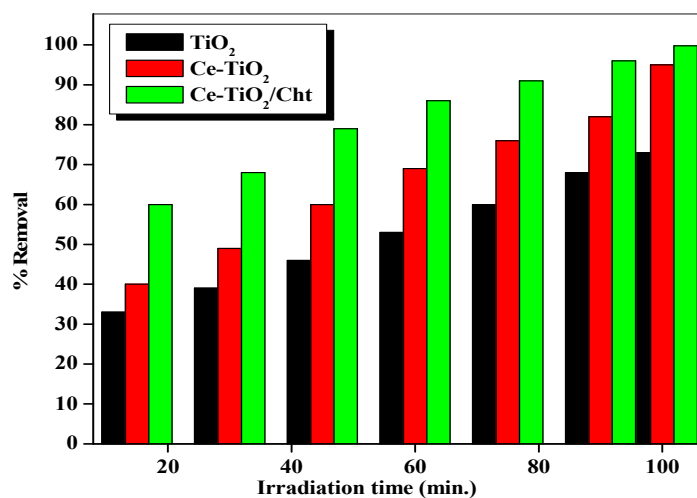


**Figure 11.** Parameters of the effect of irradiation time on RhB dye degradation under UV irradiation onto pure TiO<sub>2</sub>, Ce-TiO<sub>2</sub>, and Ce-TiO<sub>2</sub>/chitosan nanocomposite (Initial dye concentration: 40 ppm; Dose: 10 mg; pH: 6.5).

### 2.5. Assessment of Photodegradation Kinetics

Figure 12 compares the UV–Vis absorption spectrums of RhB dye with regards to changes in the irradiation time (in the range of 0–90 min) when Ce-TiO<sub>2</sub>/chitosan nanocomposite is available as a photocatalyst. As shown in the figure, the increased time frame of UV light irradiation leads to a continuous reduction in the absorbance of RhB dye with the Ce-TiO<sub>2</sub>/chitosan composite as a catalyst and the decreased absorption band intensity for the dye is an indication of the degradation process. As shown in the figure, the disappearance of RhB dye's characteristic peak at 483 nm after 100 min of UV light irradiation depicted that the dye had been degraded completely by the Ce-TiO<sub>2</sub>/chitosan composite catalyst [36]. This indicates that the Ce-TiO<sub>2</sub>/chitosan composite catalyst has greater photocatalytic activity than that of Ce-TiO<sub>2</sub>.

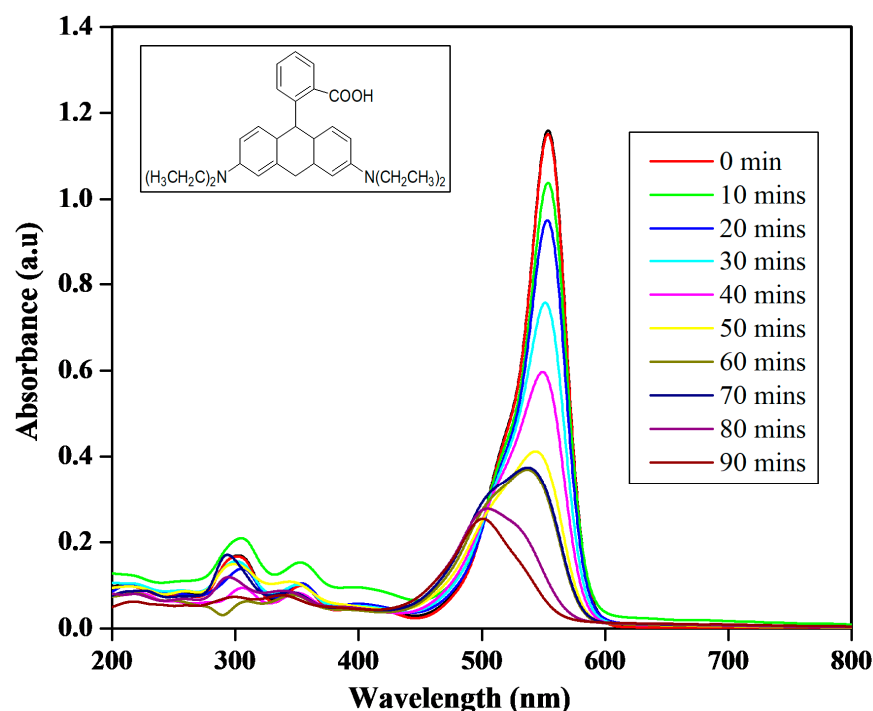


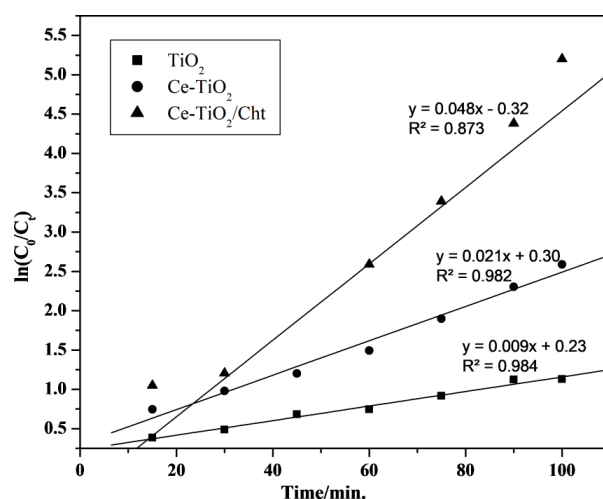
Figure 12. Comparison of changes in the UV–Vis absorption spectrum of RhB dye in the presence of Ce-TiO<sub>2</sub>/chitosan nanocomposite catalyst with varying irradiation time in the range of 0–90 min.

Figure 13 provides the comparison of photocatalytic degradation kinetics among the three catalysts of TiO<sub>2</sub>, Ce-TiO<sub>2</sub>, and Ce-TiO<sub>2</sub>/chitosan under UV light irradiation, where the reaction indicated to follow first-order kinetics of Langmuir–Hinshelwood (L-H) law of heterogeneous reaction concerning the time (*t*) of irradiation.

$$\ln \left( \frac{C_0}{C_f} \right) = K_{app} t$$

where, *C*<sub>0</sub>—initial dye concentration, *C*<sub>*f*</sub>—final dye concentration at time *t*, *t* the irradiation time, and *K*<sub>*app*</sub> the apparent first-order rate constant.

For the three catalyst samples, the values of  $\ln(C_0/C_t)$  were plotted against time (min), where the obtained plots were found to be linear (Figure 13). Table 3 provides the comparison of rate constant values obtained from the slopes of RhB degradation for TiO<sub>2</sub>, Ce-TiO<sub>2</sub>, and Ce-TiO<sub>2</sub>/chitosan composite.



**Figure 13.** Comparison of  $\ln(C_0/C_t)$  against the time interval towards RhB dye degradation under UV light irradiation for the catalyst samples of  $\text{TiO}_2$ ,  $\text{Ce-TiO}_2$ , and  $\text{Ce-TiO}_2/\text{chitosan}$ .

**Table 3.** First-order kinetic rate constant ( $k$ ) and regression coefficient ( $R^2$ ) of RhB dye degradation under UV light irradiation.

Photocatalyst	Rate Constant ( $k$ )	$R^2$
$\text{TiO}_2$	0.0207	0.907
$\text{Ce-TiO}_2$	0.0598	0.938
$\text{Ce-TiO}_2/\text{chitosan}$	0.1013	0.999

Figure 14 provides the comparison of first-order kinetic rate constants for the three sample catalysts of pure  $\text{TiO}_2$ ,  $\text{Ce-TiO}_2$ , and  $\text{Ce-TiO}_2/\text{chitosan}$ . From the comparison of results, the  $\text{Ce-TiO}_2/\text{chitosan}$  composite catalyst has a high-rate constant value as compared to the other two catalysts ( $\text{TiO}_2$  and  $\text{Ce-TiO}_2$ ), indicating the occurrence of higher photocatalytic activity towards RhB degradation under sunlight. Such an observation of enhanced catalytic activity as against pure  $\text{TiO}_2$  and  $\text{Ce-TiO}_2$  originating mainly from the active role played by both compounds of Ce and chitosan has enormous support for the upregulation of light absorption capacity and at the same time incorporating the effective mechanism of electron acceptor-transporter ability within the composite [37]. This entire phenomenon may have effectively blocked the re-accommodation of charges and stimulated the transfer of charges within  $\text{TiO}_2$ .

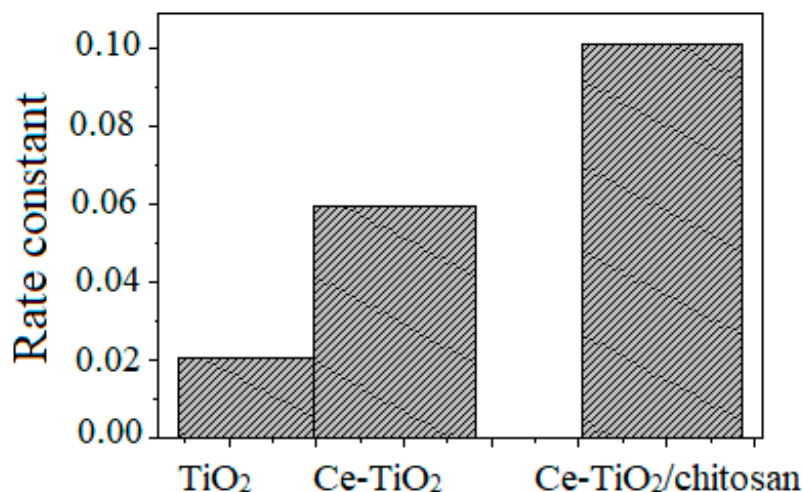


**Figure 14.** Comparison of first-order kinetic rate constant ( $k$ ) and regression coefficient ( $R^2$ ) among the samples of  $\text{TiO}_2$ ,  $\text{Ce-TiO}_2$ , and  $\text{Ce-TiO}_2/\text{chitosan}$  towards RhB dye degradation under UV irradiation.

## 2.6. Photodegradation Mechanism

In the Ce-TiO<sub>2</sub>/chitosan nanocomposite, the active photocatalytic behavior of the TiO<sub>2</sub> core can be enhanced by the availability of metal Ce as well as chitosan. In general, Ce metal and the biopolymer of chitosan have the capacity to offer multifunctional characteristics, i.e., the Ce can trap the excited electrons from the TiO<sub>2</sub> core while chitosan serves as an energy harvester so more light energy can get absorbed from the UV light source. The combination of these two phenomena like the trapping of excited electrons and the light-harvesting mechanism slows down the recombination of electron-hole and at the same time the formation of O<sub>2</sub><sup>•-</sup> gets increased which has the capacity to eventually degrade the dye pollutants, in our case the RhB dye. Oxygen molecule scavenges the electrons generated by the O<sub>2</sub><sup>•-</sup> and OH<sup>•</sup> species. The holes are attacked by the water molecule available at the valence band of core TiO<sub>2</sub> and thus support the generation of OH radicals. It acts as a strong oxidant for the complete mineralization of organic pollutants. Hence the RhB molecules in the solution can get hunted by the oxidative radicals to form some intermediate compounds, the mineralized products of non-toxic nature towards the environment and the aquatic life. The reaction mechanism is represented schematically in Figure 15 [38–40]. The following are the suggested reactions responsible for the degradation of the RhB dye using Ce-TiO<sub>2</sub>/chitosan nanocomposite.

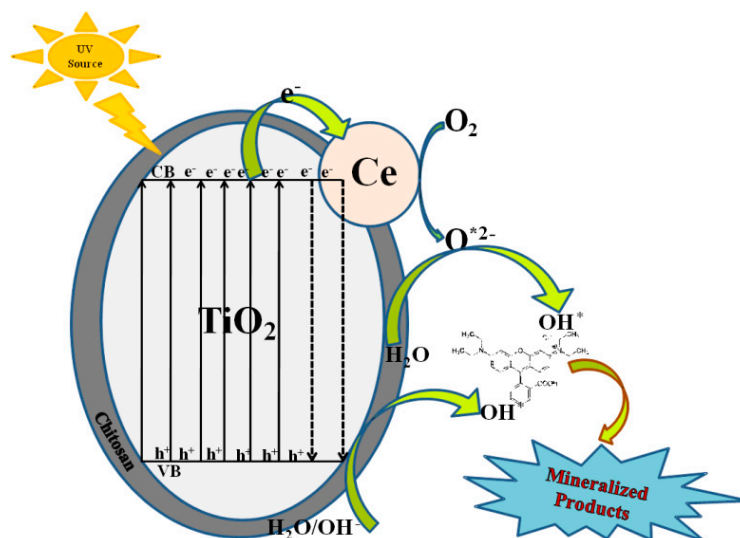
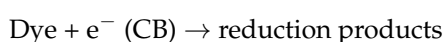
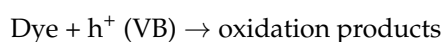
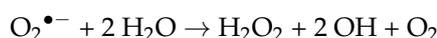
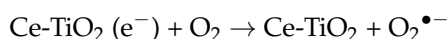
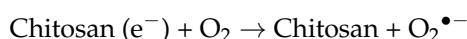
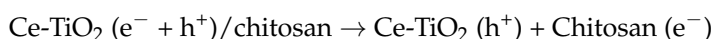


**Figure 15.** Schematic representation of the photodegradation mechanism at the surface of Ce-TiO<sub>2</sub>/chitosan nanocomposite (from the figure, \* corresponds to an excited state of oxygen).

### 3. Materials and Methods

#### 3.1. Chemicals

All chemicals such as titanium dioxide (TiO<sub>2</sub>), titanium isopropoxide (TTIP), Chitosan, Cerium nitrate Ce(NO<sub>3</sub>)<sub>2</sub>, and ethanol were purchased from Sigma–Aldrich (Bangalore, India) with 98% purity. It was used as received without further purification and the solvents used were analytical grade. Distilled water was used as a solvent in all the preparations.

#### 3.2. Synthesis of Ce-TiO<sub>2</sub> Loaded Chitosan

For the synthesis of Ce-TiO<sub>2</sub>/chitosan nanocomposite, the hydrothermal method was employed and for that, about 3 g of chitosan was dispersed in 20 mL of anhydrous ethanol in a beaker. The mixture was then stirred using a magnetic stirrer for 3 h to obtain an anhydrous suspension of chitosan. Now, 100 mL aqueous Ce(NO<sub>3</sub>)<sub>2</sub> (0.085 M) was added drop-wise to the earlier prepared chitosan suspension with continuous stirring, followed by the addition of 50 mL methanol (24.44 M) and continued the vigorous stirring for another 2 h. At this stage, a color change from white to pale yellow can be observed. To this suspension mixture, a dropwise addition of 3.5 mL of TTIP at a ratio of not exceeding 20 drops per minute was performed. After the complete addition, the magnetic stirring was maintained for another 5 h, and at the end, the precipitate of Ce-TiO<sub>2</sub> nanoparticles formed were collected by centrifugation, washed with ethanol and distilled water, and dried at 50–100 °C with the use of hot air oven. The powdered sample obtained is yellow which was subjected to calcination at 900 °C for 9 h to finally generate the faint yellow-colored product [41].

#### 3.3. Photodegradation Studies

The catalytic efficacy of our synthesized Ce-TiO<sub>2</sub>/chitosan nanocomposite under the influence of UV light was evaluated against the RhB dye degradation, following exposure to direct sunlight for a specified time interval. In this study, the stock solutions of RhB dye with required concentrations were prepared using double distilled water as solvent. For the reaction, 100 mL of the known concentration of RhB dye solution was taken in a photo reactor vessel and then added with the required amount (weighed exactly) of photocatalyst (either of TiO<sub>2</sub>, Ce-TiO<sub>2</sub>, or Ce-TiO<sub>2</sub>/chitosan nanocomposite). The reaction mixture was subjected to stirring on a magnetic stirrer for 5 min and then exposed to sunlight directly for a specific time frame. After the period, the solution mixture was collected from the reaction vessel, and the suspended solid particles were separated using centrifugation. The amount of unreacted RhB that is remaining in the solution was measured by analyzing the sample using the spectrophotometric technique, where the absorption wavelength in the range of 550–570 nm was applied on a spectrophotometer. Preliminary studies of dark experiments (without the requirement of light irradiation) were performed first to understand the time frame required to achieve the adsorption–desorption equilibrium of all the catalyst samples (TiO<sub>2</sub>, Ce-TiO<sub>2</sub>, and Ce-TiO<sub>2</sub>/chitosan) and also to define  $t = 0$  for the photocatalytic reactions (instant to turn on the irradiation). One point must be kept in mind that the RhB dye itself has some light absorption capacity to undergo self-degradation and this level is negligible as compared to the photocatalyzed RhB degradation.

The following relationship was used to calculate the extent of RhB dye that got removed (degraded) by the nanocomposite,

$$\text{Percentage (\%)} \text{ dye removal (R)} = (C_i - C_f)/C_i \times 100$$

where,  $C_i$  = initial dye concentration (in ppm);  $C_f$  = final dye concentration (ppm) at a specified time interval.

#### 3.4. Instrumental Analysis

The particle sizes and shape were analyzed using the TEM where the studies were performed on a TECNAI-G (model T-30) S-twin high-resolution transmission electron microscope (FEI Company, Hillsboro, OR, USA) operated at an accelerating voltage of

300 kV. Likewise, the surface morphological features of Ce-TiO<sub>2</sub>/chitosan nanocomposite were analyzed using the SEM analysis and for that, the HITACHI SU6600 instrument operating at an accelerating voltage of 1.5 kV (Hitachi High-Technologies Corporation, Tokyo, Japan) was employed. The surface bonding was investigated using the FTIR spectra and was recorded using BRUKER TENSOR 27 (Bruker, Billerica, MA, USA) in the wavenumber region of 4000–400 cm<sup>-1</sup>, a resolution of 4 cm<sup>-1</sup> was selected. The nature of the optical properties of the composite was studied using UV-Vis spectroscopy and for that, TECHCOMP UV-Vis 8500 double-beam spectrometer (TECHCOMP Limited, Kowloon, Hong Kong) was used. The crystallinity and crystal structure were studied using the powdered XRD and the patterns recorded at room temperature using Bruker D8 advanced X-ray diffraction system with Cu-K $\alpha$  radiation (Bruker, Billerica, MA, USA).

The experiments related to photocatalytic dye degradation under the influence of Ce-TiO<sub>2</sub>/chitosan nanocomposite were carried out by the direct exposure of sample tubes to the sunlight for specified time intervals at our college (summertime in April and May, time of 11:30 a.m. to 1:30 p.m.; Latitudes and longitudes of 9°27' N and 77°47' E respectively). Under the tested conditions, the average sunlight intensity was found to be around 1200 Wm<sup>-2</sup>. At the end of each reaction, the residual concentration of RhB dye was measured using the UV-Vis spectrophotometer (ELICO SL 207 MINI SPEC, Hyderabad, TS, India) set at the specified absorption and emission wavelengths of RhB dye. Also, the dye solution pH was measured by making use of a digital pen pH meter (Hanna instrument, Vila do Conde, Portugal).

#### 4. Conclusions

In conclusion, the nanocomposite of TiO<sub>2</sub>-Ce/chitosan was successfully fabricated using a hydrothermal process to have a high level of photocatalytic activity toward the degradation of dye pollutants released at the industrial sites. Following the physical characterization of the nanocomposite, the RhB dye degradation studies have witnessed the highly supportive nature of Ce in terms of promoting electron excitation and its transfer properties towards the base TiO<sub>2</sub>. Likewise, the availability of chitosan biopolymer in the fabricated nanocomposite has improved the active surface area and also enhanced the UV light harvesting ability of the Ce-TiO<sub>2</sub> core, where all these factors have supported a significant enhancement in the photocatalytic efficacy as against the other two catalysts of pure TiO<sub>2</sub> and bare Ce-TiO<sub>2</sub>. Overall, the results (Tauc plots) of the current study stress the importance of incorporating Ce and chitosan along with TiO<sub>2</sub> in terms of reducing the absorption wavelength and improving the porosity. Such an improvement in the functional properties of the nanocomposite can turn it into an effective photocatalyst that can degrade organic dye pollutants and sustainably purify industrial wastewater. We believe that the developed nanocomposite of biopolymer not only opens new horizons in the field of heterogeneous photocatalysis but also supports multiple applications in solar cells, biosensors, anticorrosive coatings, electro-chromic devices, etc.

**Author Contributions:** A.C.I.: conceptualization, investigation, methodology, writing—the original draft; J.R.M.: supervision, writing—review and editing; M.P.: formal analysis, resources, and data curation; F.M.: writing—review and editing, formal analysis, and funding acquisition; H.A.A.-L.: formal analysis and funding acquisition; A.A.S.: resources, data curation, and formal analysis. All authors have read and agreed to the published version of the manuscript.

**Funding:** Deputyship for Research and Innovation, "Ministry of Education" in Saudi Arabia for funding this research (IFKSUOR3-097-3).

**Data Availability Statement:** Data can be available from the first author upon official request and as per the requirement.

**Acknowledgments:** The authors extend their appreciation to the Deputyship for Research and Innovation, "Ministry of Education" in Saudi Arabia for funding this research (IFKSUOR3-097-3).

**Conflicts of Interest:** The authors declare no conflict of interest.

## References

1. Yadav, S.; Yadav, A.; Bagotia, N.; Sharma, A.K.; Kumar, S. Adsorptive potential of modified plant-based adsorbents for sequestration of dyes and heavy metals from wastewater—A review. *J. Water Process Eng.* **2021**, *42*, 102148. [[CrossRef](#)]
2. Hussain, S.; Khan, N.; Gul, S.; Khan, S.; Khan, H. Contamination of water resources by food dyes and its removal technologies. In *Water Chemistry* Edited by Murat Eyvaz and Ebubekir Yüksel; IntechOpen: London, UK, 2020; pp. 1–14. [[CrossRef](#)]
3. Naseem, T.; Durrani, T. The role of some important metal oxide nanoparticles for wastewater and antibacterial applications: A review. *Environ. Chem. Ecotoxicol.* **2021**, *3*, 59–75. [[CrossRef](#)]
4. Sikdar, P.; Uddin, M.M.; Dip, T.M.; Islam, S.; Hoque, M.S.; Dhar, A.K.; Wu, S. Recent advances in the synthesis of smart hydrogels. *Mater. Adv.* **2021**, *2*, 4532–4573. [[CrossRef](#)]
5. Raji, Z.; Karim, A.; Karam, A.; Khalloufi, S. Adsorption of heavy metals: Mechanisms, kinetics, and applications of various adsorbents in wastewater remediation—A review. *Waste* **2023**, *1*, 775–805. [[CrossRef](#)]
6. Rathi, B.S.; Kumar, P.S. Application of adsorption process for effective removal of emerging contaminants from water and wastewater. *Environ. Poll.* **2021**, *280*, 116995. [[CrossRef](#)] [[PubMed](#)]
7. Iqbal, Z.; Tanweer, M.S.; Alam, M. Recent advances in adsorptive removal of wastewater pollutants by chemically modified metal oxides: A review. *J. Water Process Eng.* **2022**, *46*, 102641. [[CrossRef](#)]
8. Liu, D.; Li, C.; Ge, J.; Zhao, C.; Zhao, Q.; Zhang, F.; Ni, T.; Wu, W. 3D interconnected g-C<sub>3</sub>N<sub>4</sub> hybridized with 2D Ti<sub>3</sub>C<sub>2</sub> MXene nanosheets for enhancing visible light photocatalytic hydrogen evolution and dye contaminant elimination. *Appl. Surf. Sci.* **2022**, *579*, 152180. [[CrossRef](#)]
9. Elwakeel, K.Z.; Elgarahy, A.M.; Khan, Z.A.; Almughamisi, M.S.; Al-Bogami, A.S. Perspectives regarding metal/mineral-incorporating materials for water purification: With special focus on Cr(vi) removal. *Mater. Adv.* **2020**, *1*, 1546–1574. [[CrossRef](#)]
10. Liu, D.; Li, H.; Gao, R.; Zhao, Q.; Yang, Z.; Gao, X.; Wang, Z.; Zhang, F.; Wu, W. Enhanced visible light photoelectrocatalytic degradation of tetracycline hydrochloride by I and P co-doped TiO<sub>2</sub> photoelectrode. *J. Hazard. Mater.* **2021**, *406*, 124309. [[CrossRef](#)]
11. Boruah, P.K.; Borthakur, P.; Das, M.R. Chapter 18—Magnetic Metal/Metal Oxide Nanoparticles and Nanocomposite Materials for Water Purification. In *Micro and Nano Technologies, Nanoscale Materials in Water Purification*; Thomas, S., Pasquini, D., Leu, S.-Y., Gopakumar, D.A., Eds.; Elsevier: Amsterdam, The Netherlands, 2019; pp. 473–503.
12. Vidhya, M.; Raja Pandi, P.; Archana, R.; Sadayandi, K.; Suresh, S.; Gunasekaran, S.; Podder, J.; Mohammad, F.; Al-Lohedan, H.A.; Oh, W.C. Comparison of sunlight-driven photocatalytic activity of semiconductor metal oxides of tin oxide and cadmium oxide nanoparticles. *Optik* **2020**, *217*, 164878.
13. Saravan, R.S.; Muthukumar, M.; Mubashera, S.M.; Abinaya, M.; Prasath, P.V.; Parthiban, R.; Mohammad, F.; Oh, W.C.; Sagadevan, S. Evaluation of the photocatalytic efficiency of cobalt oxide nanoparticles towards the degradation of crystal violet and methylene violet dyes. *Optik* **2020**, *207*, 164428. [[CrossRef](#)]
14. Subashini, A.; Prasath, P.V.; Sagadevan, S.; Lett, J.A.; Fatimah, I.; Mohammad, F.; Al-Lohedan, H.A.; Alshateet, S.F.; Oh, W.C. Enhanced photocatalytic degradation efficiency of graphitic carbon nitride-loaded CeO<sub>2</sub> nanoparticles. *Chem. Phys. Lett.* **2021**, *769*, 138441. [[CrossRef](#)]
15. Keerthana, S.P.; Yuvakkumar, R.; Ravi, G.; Hong, S.I.; Al-Sehemi, A.G.; Velauthapillai, D. Fabrication of Ce doped TiO<sub>2</sub> for efficient organic pollutants removal from wastewater. *Chemosphere* **2022**, *293*, 133540. [[CrossRef](#)] [[PubMed](#)]
16. Matějová, L.; Troppová, I.; Jankovská, Z.; Sezimová, H.; Endres, J.; Peikertová, P.; Leon, M.M.G. Ecotoxicity of TiO<sub>2</sub>, cerium and zirconium doped TiO<sub>2</sub> photocatalysts prepared by different preparation methods and using different titanium precursors. *Surf. Interf.* **2023**, *38*, 102762. [[CrossRef](#)]
17. Heydari Orojloo, S.; Rastegarzadeh, S.; Zargar, B. Experimental and modeling analyses of COD removal from industrial wastewater using the TiO<sub>2</sub>–chitosan nanocomposites. *Sci. Rep.* **2022**, *12*, 11088. [[CrossRef](#)] [[PubMed](#)]
18. Choudhary, K.; Saini, R.; Purohit, L.P. Controllable synthesis of Ce-doped ZnO: TiO<sub>2</sub> nanospheres for photocatalytic degradation of MB dye and levofloxacin under sunlight light irradiation. *Opt. Mater.* **2023**, *143*, 114167. [[CrossRef](#)]
19. Feng, X.; Li, X.; Su, B.; Ma, J. Solid-phase fabrication of TiO<sub>2</sub>/Chitosan-biochar composites with superior UV–Vis light driven photocatalytic degradation performance. *Coll. Surf.* **2022**, *648*, 129114. [[CrossRef](#)]
20. Sugashini, S.; Gomathi, T.; Devi, R.A.; Sudha, P.N.; Rambabu, K.; Banat, F. Nanochitosan/carboxymethyl cellulose/TiO<sub>2</sub> biocomposite for visible-light-induced photocatalytic degradation of crystal violet dye. *Environ. Res.* **2022**, *204*, 112047. [[CrossRef](#)]
21. Adnan, M.A.M.; Afzal, S.; Johan, M.R.; Julkapli, N.M. A comparative study on the photodegradation efficiency of TiO<sub>2</sub>–CS hybrid beads under wet and dry conditions. *Int. J. Mater. Prod. Technol.* **2022**, *65*, 67–79. [[CrossRef](#)]
22. Rosdiana, E.A.; Prasetya, N.B.A.; Gunawan, G. Synthesis and characterization of TiO<sub>2</sub>-chitosan beads and its application as a degradation agent of methylene blue. *Trends Sci.* **2023**, *20*, 6670. [[CrossRef](#)]
23. Ananya, D.; Shrivatsa, K.; Parag, R.G.; Chandrodai, A. Sonochemical synthesis of Ce-TiO<sub>2</sub> nanocatalyst and subsequent application for treatment of real textile industry effluent. *Ultrason. Sonochem.* **2023**, *96*, 106426.
24. Fernandes, Q.M.; Melo, K.R.T.; Sabry, D.A.; Sasaki, G.L.; Rocha, H.A.O. Does the use of chitosan contribute to oxalate kidney stone formation? *Mar. Drugs* **2015**, *13*, 141–158. [[CrossRef](#)] [[PubMed](#)]
25. Gwen, L.; Imelda, K.; Barry, D.; Adrienne, C.-T.; Llewellyn, R.; Peter, F.; Lisbeth, G. Interactions between alginate and chitosan biopolymers characterized using FTIR and XPS. *Biomacromolecules* **2007**, *8*, 2533–2541.

26. Wandre, T.M.; Gaikwad, P.N.; Tapase, A.S.; Garadkar, K.; Vanalakar, S.A.; Lokhande, P.D.; Sasikala, R.; Hankare, P.P. Sol–gel synthesized TiO<sub>2</sub>–CeO<sub>2</sub> nanocomposite: An efficient photocatalyst for degradation of methyl orange under sunlight. *J. Mater. Sci. Mater. Electron.* **2016**, *27*, 825–833. [[CrossRef](#)]
27. Purcar, V.; Rădițoiu, V.; Nicolae, C.A.; Frone, A.N.; Rădițoiu, A.; Raduly, F.M.; Șomoghi, R.; Gabor, R.A.; Căprărescu, S. Synthesis and morpho-structural properties of TiO<sub>2</sub>-based materials. *J. Optoelectron. Adv. Mater.* **2019**, *21*, 281–286.
28. Arshia, M.H.; Sheshmani, S.; Shahvelayati, A.S.; Hajiaghababaei, L.; Ghasri, M.R.A. Intercalated chitosan-ionic liquid ionogel in SnO nanoplate: Band gap narrow and adsorption-photodegradation process. *Int. J. Biol. Macromol.* **2023**, *234*, 123660. [[CrossRef](#)] [[PubMed](#)]
29. Mohd Adnan, M.A.; Amir, M.N.I.; Yusof Hamid, M.R.Y.; Johan, M.R.; Muhd Julkapli, N. Photoactive chitosan—titania multilayer assembly for oxidative dye degradation. *J. Mater. Sci.* **2022**, *57*, 12377–12392. [[CrossRef](#)]
30. Mohammadi, R. Highly Efficient catalyst of TiO<sub>2</sub>/chitosan for Photodegradation and Sono degradation of organic pollutants. *Chem. Rev. Lett.* **2022**, *5*, 133–140.
31. Owda, M.E.; Elfeky, A.S.; Abouzeid, R.E.; Saleh, A.K.; Awad, M.A.; Abdellatif, H.A.; Ahmed, F.M.; Elzaref, A.S. Enhancement of photocatalytic and biological activities of chitosan/activated carbon incorporated with TiO<sub>2</sub> nanoparticles. *Environ. Sci. Pollut. Res.* **2022**, *29*, 18189–18201. [[CrossRef](#)]
32. Palliyalil, S.; Chola, R.K.V.; Vigneshwaran, S.; Poovathumkuzhi, N.C.; Chelaveetil, B.M.; Meenakshi, S. Ternary system of TiO<sub>2</sub> confined chitosan–polyaniline heterostructure photocatalyst for the degradation of anionic and cationic dyes. *Environ. Technol. Innov.* **2022**, *28*, 102586. [[CrossRef](#)]
33. Tomšič, B.; Bajrič, Š.; Cergonja, K.; Čepič, G.; Gerl, A.; Varga, E.L.; Panoska, M.; Peulić, S.; Skoko, J.; Gorjanc, M.; et al. Tailoring of multifunctional cotton fabric by embedding a TiO<sub>2</sub>+ZnO composite into a chitosan matrix. *Tekstilec* **2023**, *66*, 134–147. [[CrossRef](#)]
34. Ponce, J.; Peña, J.U.A.N.; Roman, J.; Pastor, J.M. Recyclable photocatalytic composites based on natural hydrogels for dye degradation in wastewaters. *Sep. Purif. Technol.* **2022**, *299*, 121759. [[CrossRef](#)]
35. Vigneshwaran, S.; Sirajudheen, P.; Meenakshi, S. Surface activated mesoporous Ag-Fe<sub>3</sub>O<sub>4</sub> tethered chitosan nano matrix heterojunction photocatalyst for organic dyes degradation: Performance, recycling, and mechanism. *Environ. Nanotechnol. Monit. Manag.* **2022**, *17*, 100654.
36. Vo, T.L.N.; Dao, T.T.; Duong, A.T.; Bui, V.H.; Nguyen, V.H.; Nguyen, D.L.; Nguyen, D.C.; Nguyen, T.H.; Nguyen, H.T. Enhanced photocatalytic degradation of organic dyes using Ce-doped TiO<sub>2</sub> thin films. *J. Sol-Gel Sci. Technol.* **2023**, *108*, 423–434. [[CrossRef](#)]
37. Singh, H.; Bokare, A.; Kumar, A.; Trehen, R.; Sharma, A.; Kumar, D. Chapter 6—Formation of magnetite-based ceramic materials and their photocatalytic applications. In *Elsevier Series on Advanced Ceramic Materials, Advanced Ceramics for Versatile Interdisciplinary Applications*; Singh, S., Kumar, P., Mondal, D.P., Eds.; Elsevier: Amsterdam, The Netherlands, 2022; pp. 115–146.
38. Yang, Z.; Lin, Z.; Huang, J. Hierarchically structured NH<sub>2</sub>-MIL-125/TiO<sub>2</sub>/cellulose composite membranes with enhanced photocatalytic performance. *Chem. Nano Mat.* **2023**, *9*, e202200504. [[CrossRef](#)]
39. Sagadevan, S.; Lett, J.A.; Vennila, S.; Prasath, P.V.; Kaliaraj, G.S.; Fatimah, I.; Léonard, E.; Mohammad, F.; Al-Lohedan, H.A.; Alshahateet, S.F.; et al. Photocatalytic activity and antibacterial efficacy of titanium dioxide nanoparticles mediated by Myristica fragrans seed extract. *Chem. Phys. Lett.* **2021**, *771*, 138527. [[CrossRef](#)]
40. Munusamy, S.; Sivaranjan, K.; Sabhapathy, P.; Ramesh, P.S.; Narayanan, V.; Mohammad, F.; Sagadevan, S. Electrochemical and photocatalytic studies of Ta<sub>3</sub>N<sub>5</sub>-TaON-PEDOT-PANI nanohybrids. *Chem. Phys. Lett.* **2021**, *780*, 138947. [[CrossRef](#)]
41. Qutub, N.; Singh, P.; Sabir, S.; Sagadevan, S.; Oh, W.C. Enhanced photocatalytic degradation of Acid Blue dye using CdS/TiO<sub>2</sub> nanocomposite. *Sci. Rep.* **2022**, *12*, 5759. [[CrossRef](#)]

**Disclaimer/Publisher’s Note:** The statements, opinions and data contained in all publications are solely those of the individual author(s) and contributor(s) and not of MDPI and/or the editor(s). MDPI and/or the editor(s) disclaim responsibility for any injury to people or property resulting from any ideas, methods, instructions or products referred to in the content.